An absorbing boundary condition for free surface water waves

Düz, B.; Borsboom, M.J.A.; Veldman, A.E.P.; Wellens, P. R.; Huijsmans, R. H.M.

DOI
10.1016/j.compfluid.2017.05.018

Publication date
2017

Document Version
Accepted author manuscript

Published in
Computers & Fluids

Citation (APA)
Düz, B., Borsboom, M. J. A., Veldman, A. E. P., Wellens, P. R., & Huijsmans, R. H. M. (2017). An absorbing boundary condition for free surface water waves. *Computers & Fluids*, *156*, 562-578. https://doi.org/10.1016/j.compfluid.2017.05.018

An absorbing boundary condition for free surface water waves

B.Düz[a,d,*], M.J.A.Borsboom[b], A.E.P.Veldman[c], P.R.Wellens[b,d], R.H.M.Huijsmans[d]

[a]*Maritime Research Institute (MARIN), Haagsteeg 2, 6708 PM Wageningen, The Netherlands*
[b]*Deltares, P.O. Box 177, 2600 MH Delft, The Netherlands*
[c]*Institute for Mathematics and Computer Science, University of Groningen, P.O. Box 407, 9700 AK Groningen, The Netherlands*
[d]*Department of Ship Hydrodynamics, Delft University of Technology, Mekelweg 2, 2628 CD Delft, The Netherlands*

Abstract

In this paper, the use of an absorbing boundary condition (ABC) is investigated for the numerical simulation of free surface water waves. An enhanced type of an ABC based on the first- and second-order Higdon boundary conditions is presented. The numerical implementation of the ABC using a staggered grid arrangement is explained in detail. Numerical examples are provided to demonstrate the performance of the proposed boundary conditions.

Keywords: local absorbing boundary condition, regular and irregular water waves, Higdon boundary condition, dispersive effects, directional effects

1. Introduction

Since the 19th century when first wave theories were proposed, understanding the motion and behavior of the waves in nature has been a very

*Corresponding author
Email addresses: b.duz@marin.nl (B.Düz), mart.borsboom@deltares.nl (M.J.A.Borsboom), a.e.p.veldman@rug.nl (A.E.P.Veldman), p.r.wellens@tudelft.nl (P.R.Wellens), r.h.m.huijsmans@tudelft.nl (R.H.M.Huijsmans)

popular subject among researchers from various fields of science. Nevertheless, even today when we have highly capable numerical methods and computational power at our disposal, particular aspects of numerical modeling of water wave propagation remain a formidable challenge. Typically the phenomena of interest are local but embedded in a vast spatial domain; for example, the interaction between free surface waves and numerous kinds of man-made structures in the ocean. For efficient computational modeling, this vast spatial domain around the region of interest is truncated via artificial boundaries, which suggests that a compact computational domain around the structure and a residual infinite domain are introduced. At this point, one of the most elusive and difficult topics surfaces when we try to answer this question: What is the boundary condition to be imposed on these artificial boundaries in such a way that the solution in the compact domain coincides with the solution in the original domain?

In the literature the boundary conditions applied on the artificial boundaries are called by various names, such as non-reflecting, absorbing, open, transparent and radiating boundary conditions. Throughout the rest of this paper we will use the term Absorbing Boundary Condition (ABC). Several types can be listed under the wide variety of ABCs: Nonlocal, semi-local or local operators, numerical dissipation zones and Dirichlet-to-Neumann (DtN) map based conditions.

Each type of ABC has significant amount of work behind it since a large number of researchers from different fields extended earlier works in various directions over the last few decades. This has resulted in a substantially broad literature. Fortunately, there are a number of good reviews. For a review regarding only high-order local ABCs, see [19]. [18] and [52] present lengthy overviews of local and non-local ABCs along with other artificial boundary conditions. Also, [26] offers a survey of exact ABCs. [9] discusses the use of ABCs and numerical dissipation zones suitable especially for compressible turbulent shear flows. For a review of ABCs and perfectly matched layers (PML) for wave propagation problems, the reader is referred to [1]. Several techniques to absorb free surface waves are briefly discussed by [48].

In order to state our motivation for the work presented in this paper, we will first lay out some requirements which are relevant for free surface water wave simulations, coastal and offshore applications. We will walk in the footsteps of [20], and present the criteria which a new ABC is expected to fulfill. We will give our comments together with his remarks written in italic form. In the mean time we will keep in mind the work by [48] and [60]

which discuss properties of different types of ABCs with respect to a number of criteria.

1. *Well-posedness: The problem in the domain including the implementation of the ABC on the artificial boundary is well-posed.* Well-posedness of an initial-boundary value problem (IBVP) needs to be addressed before discretization, and a number of classical references are available in that regard, e.g., [37], [50] and [32]. The starting point of our work will be the Higdon ABC given in Eq. (6), and the well-posedness of the IBVP with the Higdon ABC was studied by several researchers, e.g., [31, 48, 45].
2. *Accuracy on the continuous level: The amount of spurious reflection due to the ABC is small.* Theoretically speaking it is possible to reduce the amount of reflection by setting the order of an ABC as high as possible. But is that really necessary? In numerical simulations of relevant practical situations around five percent reflection is generally acceptable since this amount is also encountered in experimental basins and flumes. Therefore it may not be necessary to apply a high-order ABC for the sake of very small amount of reflection. Hence the 1st- and 2nd-order Higdon ABCs will be the starting point in our derivation.
3. *Scheme compatibility: The ABC on the boundary is compatible with the numerical scheme used in the domain.* Overall scheme compatibility can be a strict limitation for an ABC. For example, some ABCs in the literature are applicable only in spherical coordinates, and/or in 2D and/or 3D, e.g., the Grote-Keller ABC [23, 24] is designed in spherical coordinates and is inherently 3D. For us it is of critical importance that the ABC is applicable both in 2D and 3D, and can be discretized on a rectangular Cartesian grid. In Section 3.5 we will present the ABC in discrete form, and explain how easily the ABC is incorporated into the framework of the overall numerical method.
4. *Stability: The ABC does not allow any unwanted modes which propagate into the computational domain.* Stability of an ABC, or any other boundary condition, is very critical since it provides a clear indication for a potentially successful or unsuccessful computation. For the sake of brevity, we will not discuss the stability of the proposed ABC in this paper. For that purpose the reader is referred to [12].
5. *Accuracy on the discrete level: The error due to the numerical implementation of the discrete ABC is small.* Even though an ABC is

accurate on the continuous level, it may not be so on the discrete level. [20] discusses this and reports that, for example, the Perfectly Matched Layer (PML) by [3] suffers from such an issue. In Section 4 we will present results from numerical tests, and show that the error produced by the use of the discrete ABC is at an acceptable level.

6. *Efficiency: The application of the ABC on the boundary does not increase computational cost significantly.* This is where the decision of using a local ABC rather than any other type of ABC becomes more clear. With local ABCs it is possible to locate the artificial boundary close to the area of interest, and hence reduce the amount of computational work to obtain a solution. This is not the case for some of the other ABCs, for example, with the damping layer where large zones of one or more wavelengths are usually added to the domain [59]. Such implementation requires considerable computational effort especially in 3D, which renders the method inefficient. The ABC we will present does not require a large computational effort. This will be shown in Section 3.5. This property also holds when the ABC is applied in 3D. The cost of using the ABC on the boundary is proportionate to the cost of solving the governing equations within the interior of the domain.
7. *Ease of implementation: The ABC is easy to apply, and resulting numerical code is maintainable.* Implementation of an ABC is generally not rudimentary. When several properties in this list are set out to be satisfied, the resulting ABC gradually becomes more complicated. Nevertheless we will demonstrate later in this chapter that considering the overall properties of the presented ABC, the difficulty of its numerical implementation is only commensurate.
8. *Generality: The ABC performs well in a wide variety of applications.* The ABC designed here is not a general ABC which is suitable for a large class of problems. The main focus in this work is to account for dispersive and directional effects of free surface waves in an arbitrary water depth in a 3D domain. Another goal is to design an *open* boundary condition which allows waves to travel in and out of the domain over the same boundary. This is especially needed when there is a structure in the domain. At the moment, it is not clear how to deliver this property with other type of ABCs due to the fact that an in-depth discussion on this topic has been made only by a small number of researchers, e.g., [6, 40, 53, 42, 62]. In the literature, various types of boundary conditions have been used for both wave generation

and absorption. For example, Carpenter's scheme used the radiation operator by [49], which was later replaced with the high-order operator of [29] by [43]. [40] used a sponge layer method, which increased computational cost to some extent. This method has also been successfully implemented by various researchers, e.g., [51, 16]. As a strong emphasis on efficiency is made in the sixth criterion, we realized that local operators are more suitable in developing an *open* boundary condition in an efficient manner; see [12] for further discussion on this matter. Furthermore, combined wave-current flow is an interesting challenge for any type of ABCs; work is currently underway on this topic; see [7].

The first four criteria in the list are somewhat associated with convergence of a numerical scheme. Naturally this can be demonstrated more readily once the ABC is applied. [20] states that most of the work in this field has focused on the combination of properties 5 and 6. Designing an ABC which satisfies all the criteria above remains a formidable challenge. Therefore, as many researchers, we made some compromises when it comes to some properties, and tried to deliver an ABC which accomplishes the most needed goals in an efficient manner. The novelty of the proposed ABCs lies in the properties 5, 6 and 8. Essentially, two local ABCs will be proposed that can account for dispersive and directional effects of free surface water waves in a reasonably accurate and efficient manner. The ABCs will be based on the first- and second-order Higdon operators, and only up to second-order derivatives will appear in the final discrete forms. Furthermore, the design of the ABCs will be flexible such that further improvements can be made in the future. These features will be demonstrated throughout several sections in the rest of this paper.

The absorbing boundary conditions presented in this paper have been incorporated into a numerical method called ComFLOW. ComFLOW was initially developed to simulate one-phase flow. Later, implementation of the method was extended to a wider class of problems after improving the method to model two-phase flows; see [61]. Simulation of sloshing on board spacecraft [57], [17], [55]; medical science [41], [44]; μ-gravity biology applications [46]; engineering problems in maritime and offshore industry [5], [10], [34], [36], and [39] are among those where ComFLOW has been generally used. The reader is referred to [56] and the ComFLOW website (www.math.rug.nl/∼veldman/comflow/comflow.html) for an overview of the current status of the method.

The rest of the paper is organized as follows. Section 2 presents an introduction to the topic of local absorbing boundary conditions. Design of the ABC is explained in a comprehensive manner in Section 3. After establishing the statement of the problem first, this section continues with discussions on the dispersion relation, theoretical reflection coefficient, and numerical discretization of the ABC. In Section 4 results of numerical experiments are presented in order to fully demonstrate the performance of the ABC.

2. Absorbing boundary conditions

For convenience we will present a short introduction to the first hierarchy of local absorbing boundary conditions developed by [15]. This work can be considered as one of the cornerstones in the field of absorbing boundary conditions, and is essentially related to the ABC that we will design later in this chapter. We start the discussion by considering the two dimensional wave equation

$$\frac{\partial^2 \phi}{\partial t^2} = c^2 \left(\frac{\partial^2 \phi}{\partial x^2} + \frac{\partial^2 \phi}{\partial y^2} \right) \tag{1}$$

where c is the propagation or phase speed. Solutions of this equation are plane waves which have the following form

$$\phi\left(x, y, t\right) = e^{i(k_x x + k_y y - \omega t)} \tag{2}$$

where ω is the frequency and (k_x, k_y) are the components of the wave number vector in the x- and y-directions, respectively, $\mathbf{k} = (k_x, k_y)$. Substitution of Eq. (2) in Eq. (1) results in the following expression

$$\omega^2 = c^2 \left(k_x^2 + k_y^2 \right) \tag{3}$$

which is called the dispersion relation. Left-running waves, like reflections at a right-hand side boundary at a location along the x-direction, are suppressed by demanding

$$\left(\frac{\partial}{\partial t} + c \frac{\partial}{\partial x} \right) \phi = 0. \tag{4}$$

This condition, studied by [49], has been proposed as a non-reflecting boundary condition by [15]. Higher-order versions can simply be formed by using

powers of the left-hand side operator. The 2nd-order Engquist-Majda boundary condition then takes the following form

$$\left(\frac{\partial}{\partial t}+c\frac{\partial}{\partial x}\right)^{2}\phi=0. \tag{5}$$

Switching to the three-dimensional case, [31, 33] showed that it is possible to allow the wave under an angle of incidence α with the outflow boundary. In the higher-order conditions even more angles can be chosen: α_p, $p=1,...,P$, where P is the order of the boundary condition. Higdon's condition reads:

$$\prod_{p=1}^{P}\left(\cos\alpha_p\frac{\partial}{\partial t}+c\frac{\partial}{\partial x}\right)\phi=0. \tag{6}$$

In order to assess the benefit of using Eq. (6) as opposed to Eq. (5), we need to take a look at the amount of spurious reflection generated by each scheme as a function of the angle of incidence. For this purpose we utilize the idea that at the artificial boundary, we can express the solution as the sum of outgoing and reflected waves, that is

$$\phi\left(x,y,t\right)=e^{i(k_x x+k_y y-\omega t)}+Re^{i(-k_x x+k_y y-\omega t)}, \tag{7}$$

where the first term represents the wave with amplitude equal to unity impinging on the boundary, and the second term represents the spuriously reflected wave with amplitude R. To evaluate R, we substitute Eq. (7) into the 1st- and 2nd-order Engquist-Majda boundary conditions, and arrive at the following relation

$$\begin{aligned}\left|R_{E\&M-1}\right| &= \left|\frac{1-\cos\theta}{1+\cos\theta}\right|,\\ \left|R_{E\&M-2}\right| &= \left|\frac{1-\cos\theta}{1+\cos\theta}\right|^{2}.\end{aligned} \tag{8}$$

Here $R_{E\&M-1}$ and $R_{E\&M-2}$ denote the amount of spurious reflection corresponding to the 1st- and 2nd-order Engquist-Majda boundary conditions, respectively, and θ is the 'real' angle of incidence measured in the clockwise or counter-clockwise direction from the positive x-direction, $|\theta|<\pi/2$. If Eq.

(7) is substituted into the general Higdon boundary conditions Eq. (6), the following reflection coefficient is obtained

$$|R_H| = \prod_{p=1}^{P} \left| \frac{\cos\alpha_p - \cos\theta}{\cos\alpha_p + \cos\theta} \right|. \tag{9}$$

Observing Eq. (8) it can be readily seen that the Engquist-Majda boundary conditions are non-reflecting when the waves are approaching in the normal direction to the boundary, $\theta = 0$. If the waves approach the boundary at nonnormal angles of incidence, then $|R_{E\&M-2}| < |R_{E\&M-1}|$ holds for $|\theta| < \pi/2$. When $|\theta| = \pi/2$, both boundary conditions provide full reflection. This result is of no consequence since it corresponds to the case where waves propagate parallel to the boundary, which is redundant with our discussion. On the other hand, Higdons boundary condition (6) is non-reflecting as soon as θ equals one of the $\pm\alpha_p$'s. Hence, it is possible to adapt the choice of α to any situation at hand.

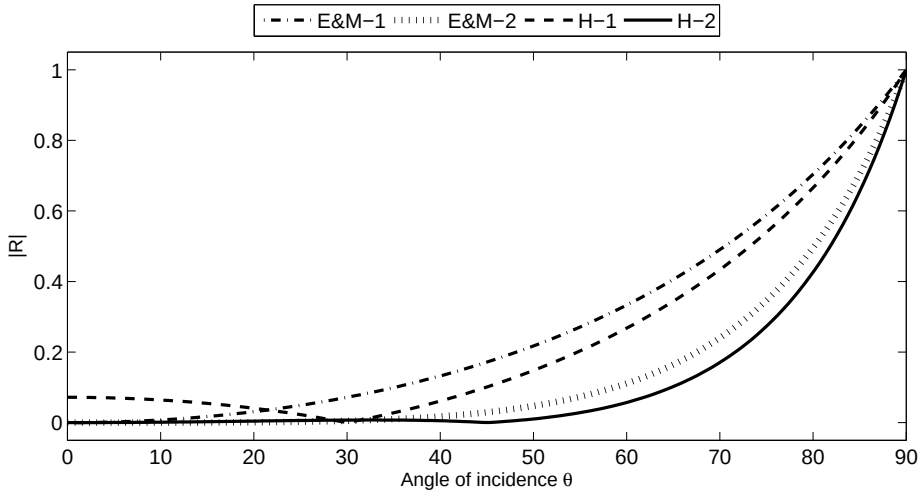

Figure 1: Reflection coefficient of four boundary conditions versus the angle of incidence. $E\&M-1$ and $E\&M-2$ stand for the 1st- and 2nd-order Enguist-Majda ABC, and $H-1$ and $H-2$ the 1st- and 2nd-order Higdon ABC. $\alpha_1 = 30°$ is chosen for the 1st-order Higdon ABC, and $\alpha_1 = 0°, \alpha_2 = 45°$ for the 2nd-order Higdon ABC.

The reflection coefficient as a function of the angle of incidence for the 1st- and 2nd-order Enguist-Majda and Higdon ABCs is illustrated in Fig.

1. Clearly the 2nd-order methods are superior to 1st-order ones. Among the four methods the 2nd-order Higdon is the most effective. The choice of $\alpha_1 = 0°, \alpha_2 = 45°$ appears to give the best overall performance for waves striking the boundary under the range of angles between $\theta = 0°$ and $\theta = 50°$.

Similar efforts have been made by other researchers to design high-order local absorbing boundary conditions. For example, [2] developed a high-order local boundary condition in spherical coordinates. Theoretically, these high-order boundary conditions have an arbitrary accuracy which increases as the order of the conditions increases. However, they include high-order spatial and temporal derivatives, which eventually compromises the locality of these conditions. Furthermore numerical implementation starts to become a serious bottleneck since discretizing an arbitrary Pth-order differential operator is unpractical. Indeed [25] notes that only up to 2nd-order conditions are most commonly used in practice. Nevertheless the above boundary conditions have been used in practical applications and satisfactory results have been achieved in many cases [20].

In order to circumvent the difficulty of having high-order derivatives associated with a high-order boundary condition, [8] introduced the use of auxiliary variables imposed on the artificial boundary. The Collino boundary condition of arbitrary order does not involve any high derivatives beyond 2nd-order. Many high-order local absorbing boundary conditions today utilize the idea of auxiliary variables as the basis in their design, e.g., [27], [21] and [29]. Thus [19] claims that [8] can be regarded as the pioneer of the *practically* high-order local absorbing boundary conditions.

In addition to directional effects of the waves, dispersion has also been the focus of many researchers. Considering the highly nonlinear governing equations which are employed in many complex modeling applications, it is unlikely to have a priori knowledge regarding the phase speed c. As a result c is generally computed during the course of the numerical simulation. [47] suggested the following idea to compute c

$$c = -\frac{\partial\phi/\partial t}{\partial\phi/\partial x}. \tag{10}$$

Clearly this expression is found from the boundary conditions (4) itself, and makes sense only in the discrete form. To discretize the right-hand side, he suggested using the information near the boundary at the previous time step via suitable finite difference approximations. An obvious problem is that we may encounter unphysical values from this computation. When the angle of

incidence increases, i.e., the waves are rather oblique, the normal derivative approaches zero, which results in an infinitely large value for c. Furthermore if $c < 0$ is obtained, then this implies that information propagates back into the domain instead of outside. If these unphysical values are in turn used with the boundary condition, numerical instability will occur. Therefore, in practice, a restriction on c is imposed for stable solutions, for example when explicit leapfrog time differencing and upstream space differencing are used in discretizing the boundary condition, then c is bounded to satisfy the CFL condition, $0 \leq c \leq \Delta t/\Delta x$. [11] investigated the use of Orlanski's scheme in numerical simulations of shallow water waves, for which c has the well-defined value of $\sqrt{gh}$. They report that the scheme rarely yields a meaningful value for c because computed values of c often fall outside the stability limit, and have to be reset to either zero or $\Delta t/\Delta x$. In the spirit of Orlanski's work various schemes have been developed to approximate c in a more accurate and stable fashion. For a survey of those schemes the reader is referred to the work of [30] and [35].

Other attempts have also been made to incorporate the dispersive nature of the free surface waves into the construction of absorbing boundary conditions. The main trend among researchers seems to be using high-order local ABCs, e.g., [22] and [28] where auxiliary variables are utilised to eliminate high-order derivatives in the high-order ABCs, see [38] for a comparison between the two works for a dispersive one-dimensional medium.

3. Design of the ABC

3.1. Statement of the problem

If we consider water as a homogeneous, incompressible, viscous fluid, we can describe fluid motion in an arbitrary domain by the continuity equation and the Navier-Stokes equations written in a conservative form as the following,

$$\oint_{\Gamma} \mathbf{u} \cdot \mathbf{n} \; d\Gamma = 0, \tag{11}$$

$$\oint_{\Omega} \frac{\partial \mathbf{u}}{\partial t} d\Omega + \oint_{\Gamma} \mathbf{u}\mathbf{u}^T \cdot \mathbf{n} d\Gamma = -\frac{1}{\rho} \oint_{\Gamma} (p\mathbf{n} - \mu \nabla \mathbf{u} \cdot \mathbf{n}) d\Gamma + \oint_{\Omega} \mathbf{F} d\Omega. \tag{12}$$

In Eqns. (11) and (12), Ω denotes a volume with boundary Γ (see Fig. 2) and normal vector $\mathbf{n}$, $\mathbf{u} = (u, v, w)^T$ is the flow velocity, ρ is the fluid density, p

is the pressure, μ is the dynamic viscosity, ∇ is the gradient operator and $\mathbf{F} = (F_x, F_y, F_z)^T$ represents external body forces acting on the fluid such as gravity, centrifugal, Coriolis and electromagnetic forces. In-depth analysis of how these equations are implemented is beyond the scope of this paper, and the reader is referred to the following works for that purpose, e.g., [58] and [36]. However, we will briefly explain the adopted solution technique since some intermediate expressions in this process will often be referred to later in the paper. In order to do so, we write the equations of motion in a schematic form

$$\text{div } \mathbf{u}^{n+1} = 0, \tag{13}$$

$$\frac{\mathbf{u}^{n+1} - \mathbf{u}^n}{\Delta t} + \frac{1}{\rho} \text{ grad } p^{n+1} = \mathbf{R}^n \tag{14}$$

where n and $n+1$ indicate the old and new time level, respectively, Δt is the time step, and $\mathbf{R}$ contains all convective, diffusive and body forces

$$\mathbf{R}^n = -\left(\mathbf{u}^n \cdot \text{grad}\right) \mathbf{u}^n + \nu \text{ div grad } \mathbf{u}^n + \mathbf{F}^n \tag{15}$$

in which ν is the kinematic viscosity. Discretizing the continuity equation (13) at the new time level ensures a divergence-free velocity field at this time level. Rearranging the terms in Eq. (14) yields

$$\mathbf{u}^{n+1} = \tilde{\mathbf{u}}^n - \frac{\Delta t}{\rho} \text{ grad } p^{n+1} \tag{16}$$

where

$$\tilde{\mathbf{u}}^n = \mathbf{u}^n + \Delta t \mathbf{R}^n. \tag{17}$$

The term $\tilde{\mathbf{u}}^n$ is often referred to as an auxiliary velocity, and calculated first in the solution process. After substituting (16) into (13), we have

$$\text{div grad } p^{n+1} = \frac{\rho}{\Delta t} \text{ div } \tilde{\mathbf{u}}^n. \tag{18}$$

Equation (18) is the Poisson equation for the pressure. Typically, this equation is solved using the SOR (Successive Over Relaxation) method such as developed by [4]. Once the pressure field is obtained, the velocity field at the new time level is calculated via Eq. (16).

In ComFLOW, the equations of motion (11) and (12) are solved in a computational domain Ω via imposing various types of boundary conditions

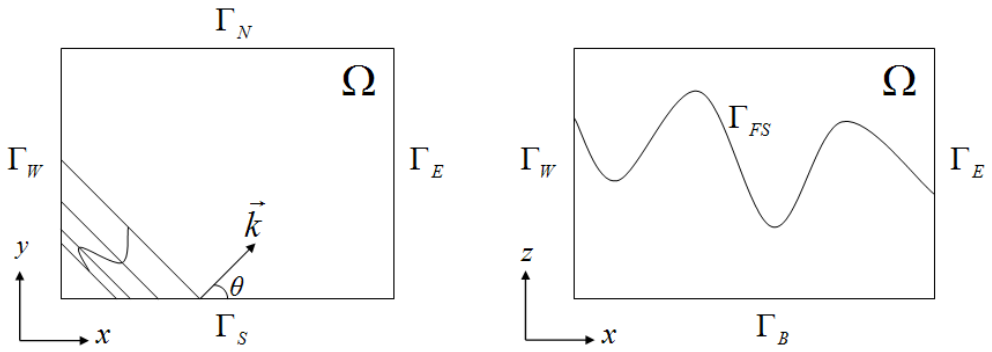

Figure 2: A computational domain with Γ_N and Γ_E as artificial boundaries.

such as free surface, wall, inflow and absorbing boundary conditions. Typically on the west and south boundaries Γ_W and Γ_S the incoming wave is prescribed. At every time level starting from $t = 0$, free surface elevations, values of the velocity components and pressure corresponding to the considered wave model are provided on Γ_W and Γ_S. At the bottom Γ_B we specify a no-slip no-penetration condition which is simply the Dirichlet condition. At the free surface Γ_{FS} continuity of normal and tangential stresses results in expressions for the velocity components and pressure. We now introduce two artificial boundaries Γ_N and Γ_E, see Fig. 2. To complete the statement of the problem, we will implement an ABC on these artificial boundaries.

3.2. ABC-1 (Dispersive ABC)

Consider the following boundary operator on Γ_E:

$$\left(\cos\alpha\frac{\partial}{\partial t} + c\frac{\partial}{\partial x}\right)\phi = 0. \tag{19}$$

[33] showed that (19) is perfectly absorbing if α is equal to the angle of incidence θ (see Fig. 2) for a wave described by the wave or velocity potential ϕ and traveling with phase speed c.

If we replace c in (19) by the dispersion relation, namely,

$$c = \sqrt{gh}\sqrt{\frac{\tanh(kh)}{kh}}, \tag{20}$$

we can rewrite (19) as

$$\left(\cos\alpha\frac{\partial}{\partial t} + \sqrt{gh}\sqrt{\frac{\tanh\left(kh\right)}{kh}}\frac{\partial}{\partial x}\right)\phi = 0. \tag{21}$$

The boundary condition (21) is perfectly absorbing for this single component, but recall that a wave is sometimes formed by superposition of a number of components. Each individual component of this wave has its own frequency, amplitude, wave number and phase. Therefore, the boundary condition (21) cannot annihilate all these wave components simply because it is evidently designed for only one of them.

At this point a question crosses one's mind: Is it possible to develop a boundary condition which has the feature of allowing reflection only to an acceptable threshold for all the components which all together form an irregular wave? One can deduce from the way this question is asked that we expect some amount of reflection for such a boundary condition but it will be restricted within certain limits.

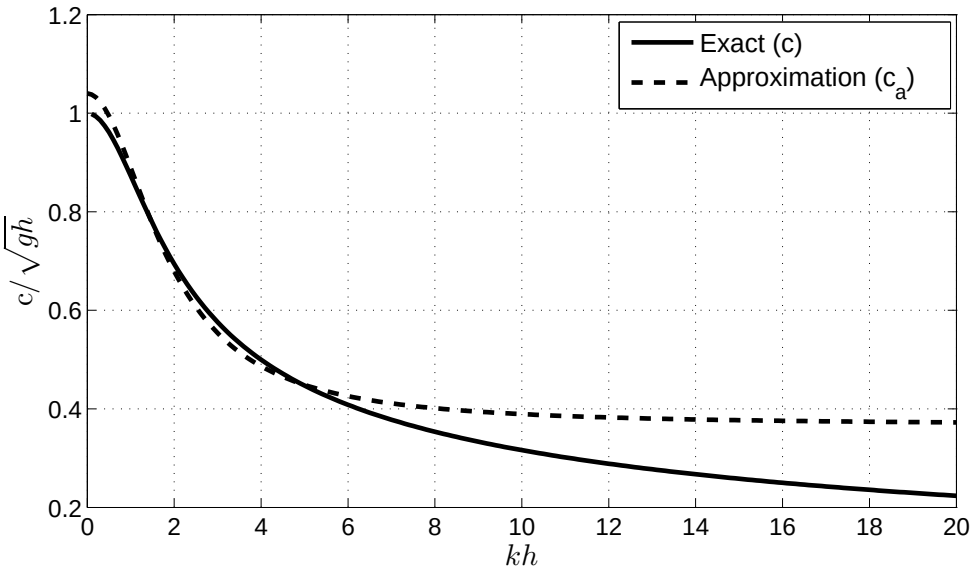

Figure 3: Approximation of the dispersion relation. For the coefficients in (22), $a_0 = 1.04$, $a_1 = 0.106$ and $b_1 = 0.289$ are used.

Now we introduce the following rational expression which approximates the dispersion relation (20),

$$c_a \approx \sqrt{gh}\frac{a_0 + a_1(kh)^2}{1 + b_1(kh)^2}, \tag{22}$$

where a proper choice of coefficients a_0, a_1 and b_1 leads to a close approximation for the largest possible range of kh values, see Fig. 3. The difference between the two curves gives an indication for the amount of reflection caused by the rational approximation. Although the accuracy of the approximation decreases for high wave numbers, eventual reflections at these wave numbers will be damped by other physical mechanisms.

Now a further improvement is introduced into the design of the boundary condition: by exploiting the approximately exponential behavior of the wave potential in the z-direction, the wave number k is computed *locally* from the potential itself. For waves of the form of $\phi \sim e^{ik(x-ct)} \cosh k(h+z)$, the following relation can be obtained

$$k^2\phi = \frac{\partial^2}{\partial z^2}\phi. \tag{23}$$

By employing (23) there is no need to choose a value for k before the numerical simulation since it is calculated during the course of the simulation. Finally we substitute (23) and (22) in (19) to reach the final form of the absorbing boundary condition to be applied on Γ_E

$$\cos\alpha \left(1 + b_1 h^2 \frac{\partial^2}{\partial z^2}\right) \frac{\partial \phi}{\partial t} + \sqrt{gh} \left(a_0 + a_1 h^2 \frac{\partial^2}{\partial z^2}\right) \frac{\partial \phi}{\partial x} = 0. \tag{24}$$

Following the same method it is easy to write the ABC on Γ_N.

3.3. ABC-2 (Dispersive directional ABC)

Now, a further modification of the dispersive ABC will be discussed to account for both dispersive and directional effects of the waves. As it was already illustrated in Fig. 1, the 2nd-order Higdon ABC has superior performance over the 1st-order one in terms of directional effects. Therefore, we will incorporate the improvements that we made in the previous section concerning dispersive effects into the 2nd-order Higdon ABC. We can write this ABC for Γ_E as the following:

$$\prod_{i=1}^{2} \left(\cos\alpha_i \frac{\partial}{\partial t} + c\frac{\partial}{\partial x}\right) \phi = 0 \tag{25}$$

where $|\alpha_i| < \pi/2$ for all i. The condition (25) is satisfied exactly by any plane wave ϕ traveling out of the domain at angles of incidence α_1 and α_2

with the phase speed c. If we expand Eq. (25), we will have

$$\left(\cos\alpha_1\frac{\partial}{\partial t}+c\frac{\partial}{\partial x}\right)\left(\cos\alpha_2\frac{\partial\phi}{\partial t}+c\frac{\partial\phi}{\partial x}\right)=0. \tag{26}$$

Considering the relations (22), (23) and (26), we realize that only one of the operators can include the approximation for the dispersion relation. Otherwise, the product of two approximations would yield a fourth-order derivative in the z-direction which will cause difficulties when discretized at the boundaries. Therefore, we substitute the relations (22) and (23) in one of the operators. The resulting expression for the ABC-2 is the following

$$\left(\cos\alpha_1\frac{\partial}{\partial t}+c\frac{\partial}{\partial x}\right)\left(\left(1+b_1h^2\frac{\partial^2}{\partial z^2}\right)\cos\alpha_2\frac{\partial\phi}{\partial t}+\sqrt{gh}\left(a_0+a_1h^2\frac{\partial^2}{\partial z^2}\right)\frac{\partial\phi}{\partial x}\right)=0. \tag{27}$$

Analogous with the discussion for the ABC-1, this expression can also be easily written for the boundary operator to be applied on Γ_N. In what follows, we will demonstrate the effectiveness of the four boundary conditions, Eqs. (19), (24), (25) and (27), by displaying the amount of reflection as a function of both the angle of incidence θ and the dimensionless wave number kh.

3.4. Reflection coefficients of the absorbing boundary conditions

Substituting the potential function (7) into the four boundary conditions, namely Eqs. (19), (24), (25) and (27), yields the following expressions for the reflection coefficient

$$R_{Higdon-1}=-\frac{c^{out}\cos\alpha-c\cos\theta}{c^{out}\cos\alpha+c\cos\theta}, \tag{28}$$

$$R_{Higdon-2}=-\prod_{i=1}^{2}\left(\frac{c^{out}\cos\alpha_i-c\cos\theta}{c^{out}\cos\alpha_i+c\cos\theta}\right), \tag{29}$$

$$R_{ABC-1}=-\frac{\left(1+b_1(kh)^2\right)c^{out}\cos\alpha-\sqrt{gh}\left(a_0+a_1(kh)^2\right)\cos\theta}{\left(1+b_1(kh)^2\right)c^{out}\cos\alpha+\sqrt{gh}\left(a_0+a_1(kh)^2\right)\cos\theta}. \tag{30}$$

$$R_{ABC-2}=-\left[\frac{c^{out}\cos\alpha_1-c\cos\theta}{c^{out}\cos\alpha_1+c\cos\theta}\right]\left[\frac{c^{out}\cos\alpha_2-\sqrt{gh}\frac{\left(a_0+a_1(kh)^2\right)}{\left(1+b_1(kh)^2\right)}\cos\theta}{c^{out}\cos\alpha_2+\sqrt{gh}\frac{\left(a_0+a_1(kh)^2\right)}{\left(1+b_1(kh)^2\right)}\cos\theta}\right]. \tag{31}$$

Here c^{out} denotes the phase speed of the outgoing wave, whereas c, which approximates c^{out}, is a parameter in the operators. If c and c^{out} are equal to each other, then the reflection coefficient will depend only on wave direction. In this case if the wave direction θ is equal to the angle parameter in the operators α, then all the operators will be perfectly absorbing. This suggests that since both the effects of wave direction and phase speed contribute to the amount of reflection, we need to possess information *a priori* about both parameters for small reflection. In many practical situations, however, we unfortunately have information on neither of them at outflow boundaries.

Figure 4 demonstrates the amount of reflection as a function of the angle of incidence θ and the dimensionless wave number kh to compare the effectiveness of the four boundary conditions; the first-order and second-order Higdon operators, ABC-1 and ABC-2. For the coefficients in (22) we take $a_0 = 1.04$, $a_1 = 0.106$ and $b_1 = 0.289$ while respecting the stability limits concerning these coefficients and providing a good approximation for the kh values from 0 to 20. We also take $c = 0.316\sqrt{gh}$ in the boundary conditions in which this parameter appears. This choice corresponds to the kh value of 10 which is exactly in the middle of the considered kh range between 0 and 20. All the angle parameters in the boundary conditions are set to be zero as an arbitrary initial choice.

In Fig. 4, light-colored areas between isolines illustrate small reflection zones while as the color gets darker the amount of reflection increases since grazing incidence is approached where waves propagate parallel to the outflow boundary. More particularly, white-colored zones demonstrate the ranges where the reflection coefficient is below five percent which is an acceptable threshold in practical wave simulations. Close examination of the results clearly shows the relative merits of the ABC-1 and ABC-2 over the first-order and second-order Higdon operators. The first-order Higdon operator generates reflection below five percent between kh values of 8 to 12 approximately, which is expected since the prespecified c value corresponds to the kh value of 10. However, this range is between 0 to 8 with the ABC-1. The reason for this behavior lies in the way the dispersion relation is approximated. The area between the two curves in Fig. 3 gives an indication of the amount of reflection caused by the approximation. From this plot, we clearly see that the dispersion relation is approximated well in the range $kh \in (0, 8]$. From 8 to 20, the reflection increases as the approximation becomes gradually poor, which is shown in Fig. 4(b). In terms of directional effects, the performance of the ABC-1 is somewhat better than that of the first-order

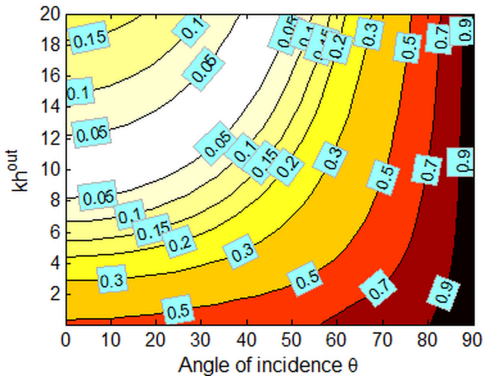

(a) First-order Higdon in Eq. (19). Corresponding reflection coefficient is Eq. (28).

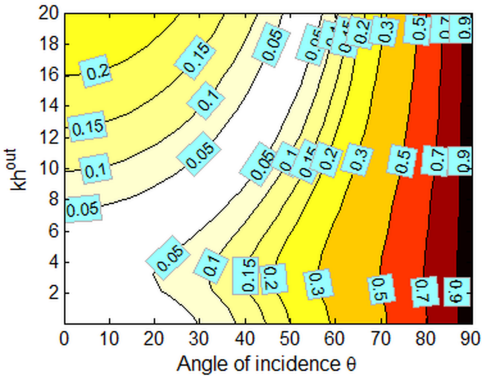

(b) ABC-1 in Eq. (24). Corresponding reflection coefficient is Eq. (30).

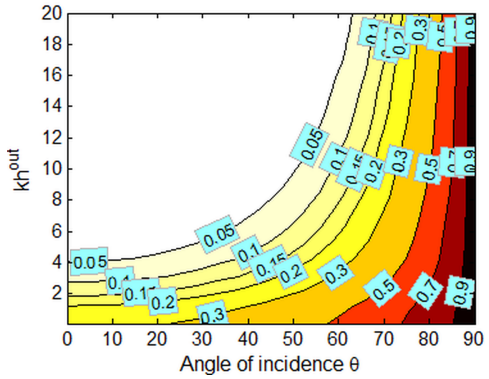

(c) Second-order Higdon in Eq. (25). Corresponding reflection coefficient is Eq. (29).

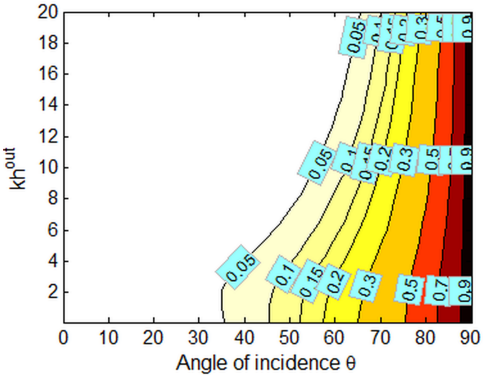

(d) ABC-2 in Eq. (27). Corresponding reflection coefficient is Eq. (31).

Figure 4: Amount of reflection (in percent) as a function of the angle of incidence θ and kh when various boundary conditions are used. In the first-order boundary conditions $\alpha = 0$ is used, and in the second-order boundary conditions $\alpha_1 = \alpha_2 = 0$ is used. Also, $c = 0.316\sqrt{gh}$ is taken in all the boundary conditions. Reflection values are written on the contour lines.

Higdon operator.

The second-order Higdon operator improves both the dispersive and directional behavior of the first-order operator. This is a result of the fact that the reflection coefficient of the second-order Higdon operator (29) is a product of two factors. Since each of these factors is smaller than 1, the product

of them becomes even smaller, and areas indicating small reflections increase, see Fig. 4(c). However, between kh values of 0 to 4, the second-order Higdon operator has a poor performance. This is where the approximation for the dispersion relation once again plays a role, and the ABC-2 consequently eliminates this poor performance. Furthermore, with ABC-2, it is possible to get low amount of reflection for kh values larger than 20 as well with a proper set of parameters.

The distinguishing characteristic of generating small reflection for a wide range of both kh values and angles of incidence reveals the reason of applying the approximation for the dispersion relation into the second-order Higdon operator: we have improved the dispersive behavior of the operator through the approximation for the dispersion relation while the operator itself has already favourable behavior in terms of directional effects. Thus, the ABC-2 becomes a versatile and accurate boundary condition for various sea states which possess both dispersive and directional features.

3.5. Numerical discretization of the ABC-1 and ABC-2

Since the governing equations inside the computational domain are written in terms of the velocity components and pressure, the ABCs (24) and (27) must be interpreted in terms of the same variables. As we have a staggered grid arrangement for the flow variables inside grid cells (see Fig. 5), the location of the outflow boundary must also be specified appropriately.

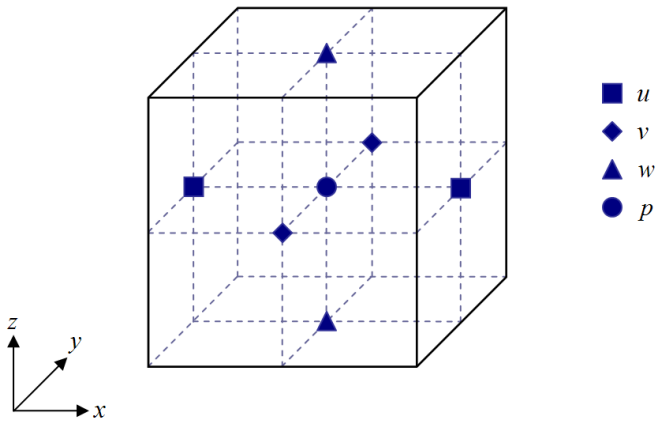

Figure 5: Locations of the velocity components and pressure in a grid cell based on the staggered grid arrangement.

All flow variables that we need here can be calculated by taking derivatives of the wave potential. Exploiting the potential theory and linearized Bernoulli equation, it is possible to obtain the following expressions for the derivatives of the wave potential with respect to time and space

$$\frac{\partial \phi}{\partial x} = u_b, \tag{32}$$

$$\frac{\partial \phi}{\partial t} = -\frac{p_b}{\rho} - g z_p. \tag{33}$$

In Eqs. (32) and (33), the subscript b indicates that the quantity is defined at the boundary, the subscript p indicates that the quantity is evaluated at the elevation of the pressure point, and for simplicity the fluid density is taken to be one. We see that both the velocity and pressure are defined at the same position in space in order to avoid any phase shift errors between flow variables. By the same logic, these variables are also defined at the same instant in time, which is the new time level t^{n+1}.

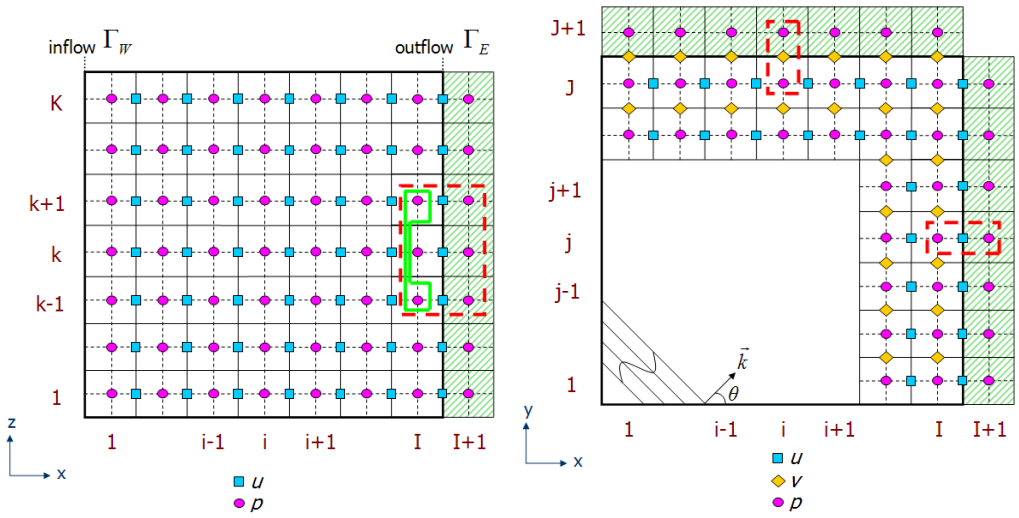

(a) Stencil of the ABC-1 in the x-z domain.

(b) Stencil of the ABC-1 in the x-y domain (top view).

Figure 6: Stencil of the ABC-1 in space

The outflow boundary is situated at the same position as u_I along the x-direction, therefore we can impose

$$u_{b,k} = u_{I,k}^{n+1} \tag{34}$$

for $k = 1, ..., K$. In order to obtain p_b, however, we employ linear interpolation and introduce mirror cells adjacent to the outflow boundary (see Fig. 6), i.e.,

$$p_{b,k} = \frac{p_{I,k}^{n+1} + p_{I+1,k}^{n+1}}{2} \tag{35}$$

for $k = 1, ..., K$. The shaded areas around the computational domain illustrated in Fig. 6 contain the mirror cells.

In order to plug the ABC-1 into the pressure Poisson equation (18) which is solved inside the computational domain for the pressure at the new time step p^{n+1}, the velocity component at the new time step u^{n+1} should be eliminated. Utilizing the discrete form of the x-momentum equation (16), we have

$$u_{I,k}^{n+1} = \tilde{u}_{I,k}^{n} - \frac{\Delta t}{\Delta x_{p_{I+1}}} \left(p_{I+1,k}^{n+1} - p_{I,k}^{n+1} \right), \tag{36}$$

u^{n+1} is written in terms of the pressure p^{n+1} and the auxiliary velocity $\tilde{u}^n$ (17). As a result, the ABC-1 will have the same temporal character as the pressure Poisson equation. Consequently, we obtain the discrete form of the ABC-1 to be prescribed on Γ_E as follows

$$\begin{aligned}
&\left[\frac{1}{2} \cos\alpha + a_0 \sqrt{gh} \frac{\Delta t}{\Delta x_{p_{I+1}}} + \left(\frac{1}{2} b_1 h^2 \cos\alpha + a_1 h^2 \sqrt{gh} \frac{\Delta t}{\Delta x_{p_{I+1}}} \right) \frac{\partial^2}{\partial z^2} \right] p_{I+1,k}^{n+1} \\
&+ \left[\frac{1}{2} \cos\alpha - a_0 \sqrt{gh} \frac{\Delta t}{\Delta x_{p_{I+1}}} + \left(\frac{1}{2} b_1 h^2 \cos\alpha - a_1 h^2 \sqrt{gh} \frac{\Delta t}{\Delta x_{p_{I+1}}} \right) \frac{\partial^2}{\partial z^2} \right] p_{I,k}^{n+1} \\
&= \left(a_0 \sqrt{gh} + a_1 h^2 \sqrt{gh} \frac{\partial^2}{\partial z^2} \right) \tilde{u}_{I,k}^{n} - g z_{p_k} \cos\alpha
\end{aligned} \tag{37}$$

for $k = 1, ..., K$ where $\Delta x_{p_{I+1}} = x_{p_{I+1}} - x_{p_I}$. Equation (37) does not contain any flow variables from the neighboring cells along the y-direction. Therefore, for simplicity, we ignored the subscript j for the flow variables here and elsewhere. For the approximation of the second-order derivative in the z-direction, the following relation designed for a stretched grid is employed,

$$\frac{\partial^2 p_k}{\partial z^2} = \frac{\Delta z_{p_k} p_{k+1} - \left(\Delta z_{p_{k+1}} + \Delta z_{p_k} \right) p_k + \Delta z_{p_{k+1}} p_{k-1}}{\frac{1}{2} \Delta z_{p_{k+1}} \Delta z_{p_k} \left(\Delta z_{p_{k+1}} + \Delta z_{p_k} \right)} \tag{38}$$

where $\Delta z_{p_{k+1}} = z_{p_{k+1}} - z_{p_k}$, and Δz_{p_k} is calculated similarly. [54] shows that the approximation (38) is second-order accurate on smoothly stretched grids.

Following the same steps, we can easily derive the ABC-1 on Γ_N. The discrete ABC-1 on Γ_E and Γ_N is a set of equation for the pressure values in the mirror cells adjacent to the computational domain, see Fig. 6. The addition of these mirror cells to the domain actually represents the cost of implementing the ABC-1. In fact, the ABC-1 is solved for pressure values in a total number of $(I + J) \times K$ cells. The stencil for $p^{n+1}_{I+1,k}$ is plotted by a red dashed line in Fig. 6(a). Observing Figs. 6(a) and 6(b) we realize that a typical stencil for a pressure point encompasses 9 flow variables, 6 of which reside in the computational domain whereas 3 can be associated with the treatment of the boundary condition.

Analogous with the discretization for the ABC-1, we follow the same steps to obtain the discrete form of the ABC-2. The derivatives of the pressure with respect to time and space are taken as

$$\frac{\partial p_b}{\partial t} = \frac{p^{n+1}_b - p^n_b}{\Delta t}, \tag{39}$$

$$\frac{\partial p_b}{\partial x} = \frac{(p_{I+1,k} - p_{I,k})^{n+1}}{\Delta x_{p_{I+1}}}. \tag{40}$$

Using the linear interpolation of the pressure values on either side of the boundary, the following expression for the final form of (39) can be obtained

$$\frac{\partial p_b}{\partial t} = \frac{(p_{I+1,k} + p_{I,k})^{n+1} - (p_{I+1,k} + p_{I,k})^n}{2\Delta t}. \tag{41}$$

Similarly, the derivatives of the velocity component with respect to time and space can be obtained, more details can be found in [12]. Upon substitution of Eqs. (40) and (41) and derivatives of velocity into (27), the final

discrete form of the ABC-2 becomes

$$\begin{aligned}
&\left[\chi+\varsigma\Delta t a_0+\vartheta+\frac{\gamma a_0}{\Delta x_{p_{I+1}}}+\left(\chi b_1+\varsigma\Delta t a_1+\vartheta b_1+\frac{\gamma a_1}{\Delta x_{p_{I+1}}}\right)\frac{h^2\partial^2}{\partial z^2}\right]p_{I+1,k}^{n+1}\\
&+\left[\chi-\varsigma\Delta t a_0-\vartheta-\gamma\xi a_0+\left(\chi b_1-\varsigma\Delta t a_1-\vartheta b_1-\gamma\xi a_1\right)\frac{h^2\partial^2}{\partial z^2}\right]p_{I,k}^{n+1}\\
&+\left[\frac{\gamma a_0}{\Delta x_{p_I}}+\frac{\gamma a_1}{\Delta x_{p_I}}\frac{h^2\partial^2}{\partial z^2}\right]p_{I-1,k}^{n+1}\\
&=\left[\chi+\chi b_1\frac{h^2\partial^2}{\partial z^2}\right]\left(p_{I+1,k}+p_{I,k}\right)^n-\left[\varsigma a_0\Delta x_{p_{I+1}}+\varsigma a_1\Delta x_{p_{I+1}}\frac{h^2\partial^2}{\partial z^2}\right]u_{I,k}^n\\
&+\left[\varsigma a_0\Delta x_{p_{I+1}}+\frac{\gamma a_0}{\Delta t}+\left(\varsigma a_1\Delta x_{p_{I+1}}+\frac{\gamma a_1}{\Delta t}\right)\frac{h^2\partial^2}{\partial z^2}\right]\tilde{u}_{I,k}^n-\left[\frac{\gamma}{\Delta t}+\frac{\gamma a_1}{\Delta t}\frac{h^2\partial^2}{\partial z^2}\right]\tilde{u}_{I-1,k}^n
\end{aligned}\tag{42}$$

for $k=1,...,K$ where

$$\chi=\frac{\cos\alpha_1\cos\alpha_2}{2\Delta t},$$

$$\vartheta=\frac{c\cos\alpha_2}{\Delta x_{p_{I+1}}},$$

$$\varsigma=\frac{\cos\alpha_1\sqrt{gh}}{\Delta x_{p_{I+1}}\Delta t},$$

$$\gamma=\frac{c\Delta t\sqrt{gh}}{\Delta x_{u_I}},$$

$$\xi=\frac{1}{\Delta x_{p_I}}+\frac{1}{\Delta x_{p_{I+1}}}.$$

Analogous with the case for the ABC-1, Eq. (42) is in fact solved for the pressure values in the mirror cells adjacent to the computational domain. Figure 7 shows the stencil $p_{I+1,k}^{n+1}$ encompassing 15 solution variables keeping in mind that the second-order vertical derivative in the z-direction is approximated with the relation (38) using a three-point variable group.

Compared to that of the ABC-1, the stencil for the ABC-2 becomes larger and extends in the direction normal to the outflow boundary. However, the cost of implementing the ABC-2 is the same as the ABC-1: Eq. (42) is solved in the same total number of $(I+J)\times K$ cells. This is clearly advantageous

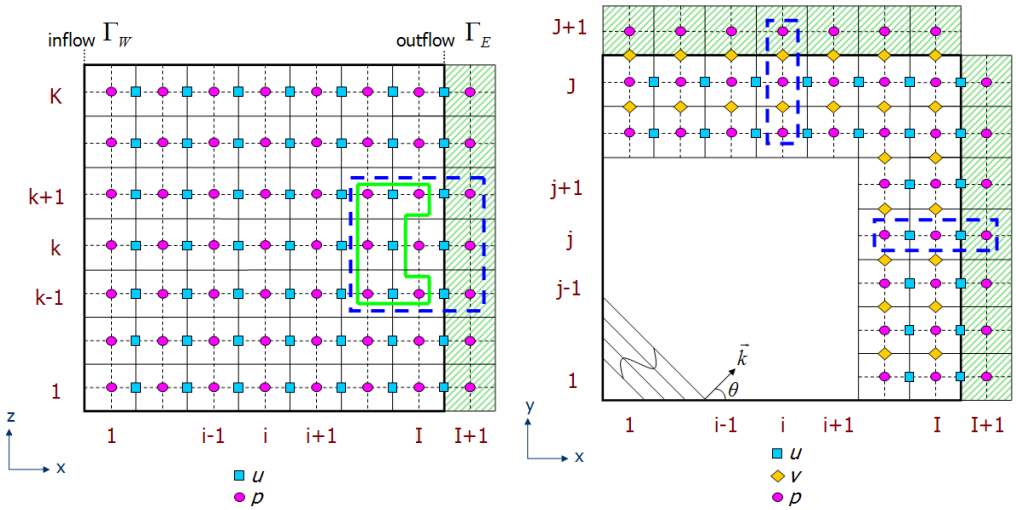

(a) Stencil of the ABC-2 in the x-z domain. (b) Stencil of the ABC-2 in the x-y domain (top view).

Figure 7: Stencil of the ABC-2 in space.

compared to numerical dissipation zones such as damping layer, as the increase in the size of the computational domain is substantially small: one layer of mesh cells are added to the outflow boundaries of the computational domain in the case of the ABCs whereas large zones of several wavelengths [59] are usually added to the domain when damping layer is employed. [59] mentions that the size of the damping layer is generally two or three times the wavelength. Considering previous numerical simulations of waves or wave-structure interactions where an absorbing boundary condition is applied in the domain [14, 13], the recommended size of the numerical damping zone is even larger than the actual computational domain itself. [59] also states that, for small reflection, numerical dissipation zones can be used in combination with absorbing boundary conditions, which increases computational cost even further.

The pressure values within the areas enclosed by the green lines in Figs. 6(a) and 7(a) do not exist in the standard stencil of the pressure Poisson equation. Hence, the large stencils of the ABCs are not suitable for a typical SOR solver [4] designed for the Poisson equation. To solve the pressure Poisson equation, therefore, we employed a Krylov subspace solver: BiCGSTAB. As preconditioner ILU(p) factorization is implemented, where the approximate

LU-decomposition is chosen more accurate near the boundary.

It should be noted that Eqs. (37) and (42) are the discretized forms of Eqs. (24) and (27), and are the results of a series of choices made within the framework of the solver at hand. For other solvers or flow models, the resulting discrete forms might differ since the intermediate steps in the discretization process might vary. The starting points to implement the ABCs are Eqs. (24) and (27). Then the question becomes how to treat the derivatives of the velocity potential, in particular the temporal derivative, and subsequently how to treat the second-order derivative in the vertical direction. Here, the temporal derivative of the velocity potential is taken using the linearized Bernoulli equation, where the quadratic velocity terms are ignored. However, adopting the linearized Bernoulli equation is not an essential requirement, and this decision was made to keep the ABCs initially less complex. In fact, future work will focus on including the quadratic terms in the Bernoulli equation, and investigating the effects of this extension on the performance of the ABCs. Furthermore, the second-order derivative in the vertical direction, for example Eq. (38), may cause issues when implemented at the bottom and free surface. Applying one-sided second-derivatives at these cells resulted in unstable simulations. At the bottom, hydrostatic pressure variation and no variation in the horizontal velocity can be assumed. This suggests

$$p_{b,0} = p_{b,1} + g z_{p_0}, \quad u_{b,0} = u_{b,1}, \tag{43}$$

keeping in mind the index notation in Fig. 7. At the free surface, the first- and second-order Higdon operators can be considered in order to avoid the second-order derivative, i.e., Eqs. (19) or (26).

Since the proposed ABCs are local where the phase speed is estimated with the Pade approximation utilizing local flow solution, they can be used in cases with varying bathymetry. In problems where different flow directions are expected, the second-order variant, ABC-2, is a better choice because it has more favorable properties especially with respect to directional effects. It should be noted that both ABCs do not account for nonlinear effects due to several assumptions made in their designs. This also holds for cases where varying bathymetry results in a strong nonlinearity in the flow.

4. Results and discussions

In this section we present results of two numerical experiments where the ABCs are applied at the outflow boundaries of the computational domain.

We will first investigate the capability of the ABCs in a test where a short-crested wave is generated in the computational domain. In the second test, circular concentric waves are generated as a result of an oscillating solid sphere impacting on water surface in a tank.

The results of the numerical simulations will be analyzed through error norms. For that purpose, we introduce three error measures,

$$e(i,j) = \eta_s(i,j) - \eta_r(i,j), \tag{44}$$

$$e_\Omega = \sqrt{\frac{1}{I}\frac{1}{J}\sum_{i=1}^{I}\sum_{j=1}^{J}\left(\eta_s\left(i,j\right) - \eta_r\left(i,j\right)\right)^2}, \tag{45}$$

$$\left\|e\right\|_\infty = \max_{i=1,2,\ldots,I}\max_{j=1,2,\ldots,J}\left\{\left|\eta_s\left(i,j\right) - \eta_r\left(i,j\right)\right|\right\}, \tag{46}$$

where η is the free surface elevation. Here the subscript s indicates the solution in the domain of interest or 'small domain' and the subscript r indicates the reference solution. In the numerical experiments considered here, the reference solution is obtained by solving the problem in a much larger domain with the same discretization in space and time. More information on the setup of the tests is given below.

The pointwise error $e\left(i,j\right)$ provides information at particular time instances throughout the simulation. In addition, it demonstrates the exact location of the error in the computational domain which is not the case for the other error measures. The common property of the global norm e_Ω (also used by [22]) and the infinity norm $\left\|e\right\|_\infty$ is that they display a complete picture of the error behavior in a single plot. More particularly, we can examine the normalized length of the error vector using e_Ω, whereas $\left\|e\right\|_\infty$ captures the maximum value in the error vector which is useful especially to check if a certain limit for the error is breached.

4.1. Short-crested wave test

In this numerical experiment, the ABCs are applied in a computational domain where a directional irregular wave is generated. The reference solution used in the error measures is computed by solving the problem in a vast domain Ω_L which is larger than the small domain Ω_S only on the x-y plane, see Fig. 8 for the illustration of the problem. The size of Ω_L is defined in such a way that the reflected waves from the outflow boundaries, which are located at $x = 250m$ and $y = 250m$, do not reach Ω_S during the simulation.

This procedure guarantees that in Ω_L, the solution in the part which has the size of Ω_S will not be perturbed by the reflected waves, and hence it can be used as a reference solution. This test combines the two effects, directional and dispersive effects, since the wave is composed of a large number of components each with its own frequency and propagation direction. Since the phase speed and the angle of incidence of the wave which is impinging on the outflow boundaries are not known beforehand, the parameters in the ABCs are chosen in such a way that the reflection coefficient is minimum for the ranges of kh and θ of the components.

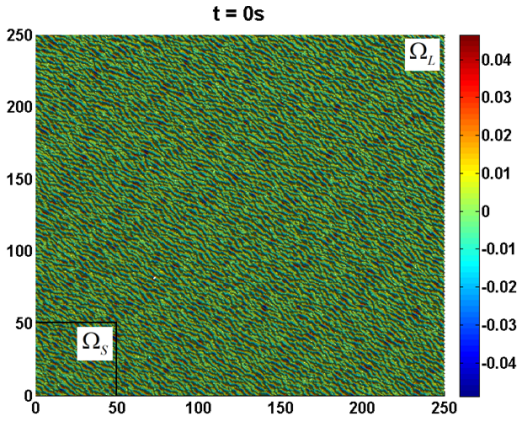

Figure 8: The setup for the short-crested wave simulation. The solution in Ω_L is considered as the reference solution.

The free surface of the short-crested wave at $t = 0s$ is shown in Fig. 9(a). This JONSWAP spectrum wave is composed of 537 Fourier components with $T_p = 9s$ and $H_s = 0.1m$, and Fig. 9(b) illustrates how the energy of this wave spreads along frequency and direction. Frequencies are defined between 0.5 and 1.4 Hz, and directions are defined between 10 and 100 degrees.

Numerical simulation is carried out by performing 4000 time-steps at $\Delta t = 0.009s$. The lengths of Ω_S in the x- and y-directions are the same, $l_x = l_y = 50m$, and the water depth is $h = 2.875m$. By running the simulations for $t_{max} = 36.0s$ and taking into account the phase speed of the fastest propagating wave component $\sqrt{gh}$, we calculate the lengths of Ω_L in the x- and y-directions as $L_x = L_y = 250m$. Two uniform grid resolutions are considered: $0.5m$ and $0.25m$.

Figure 10 shows the infinity norm $\|e\|_\infty$ and the global norm e_Ω on two grid resolutions for the two ABCs. The largest value of $\|e\|_\infty$ for the ABC-1 is

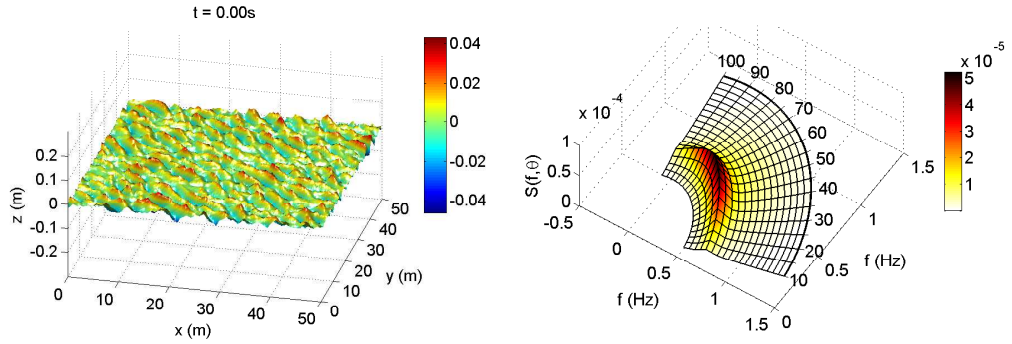

(a) The initial condition for the short-crested wave simulation in Ω_S

(b) The directional spectrum of the short-crested wave

Figure 9: Properties of the short-crested wave

nearly 21.0% whereas it is only 11.0% with the ABC-2. $\|e\|_\infty$ demonstrates a highly erratic behavior with ABC-1, it reaches the value of 11.0% at $t = 12.0s$, changes to 21.0% at $t = 23.0s$, and decreases back to 9.0% at $t = 30.0s$. When it comes to ABC-2, however, it oscillates within a much more limited band of 7.0% to 11.0% during the entire simulation.

Figure 11 demonstrates the pointwise error $\|e\,(i,j)\|$ (44), normalized with H_s and averaged over time, on the fine grid. Analogous to the previous numerical tests, the reflected waves propagate back into the computational domain and spoil the solution. As the short-crested wave striking the outflow boundaries is composed of many components propagating in their own directions, the reflected wave is so as well. It is obvious that the second-order ABC-2 is significantly better than its first-order counterpart ABC-1 (note the difference in color scale). The maximum time-averaged error from ABC-1 is nearly twice as large as that from ABC-2. Moreover, the parts of the domain which are occupied by large errors are bigger with ABC-1 than with ABC-2. This outcome also manifests itself in the global norm e_Ω in Fig. 10(b), where ABC-1 results in larger error values than ABC-2.

A common result from both boundary conditions is that large errors occupy only small parts of the domain; thus, e_Ω has much smaller values than $\|e\|_\infty$ for both ABCs. For example, the largest value of e_Ω is about 1.6% with ABC-2 on the fine grid whereas the maximum of $\|e\|_\infty$ is 11.0%.

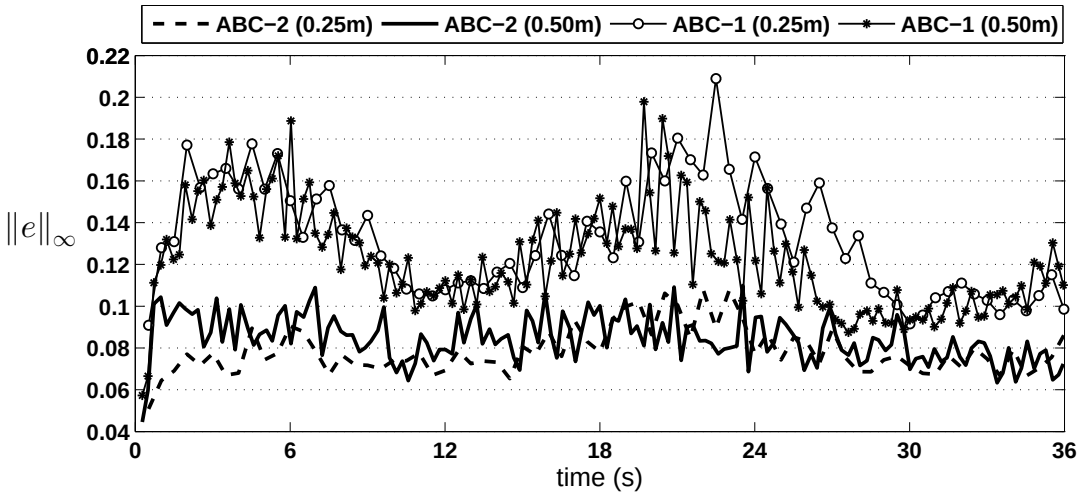

(a) The infinity norm $\|e\|_\infty$

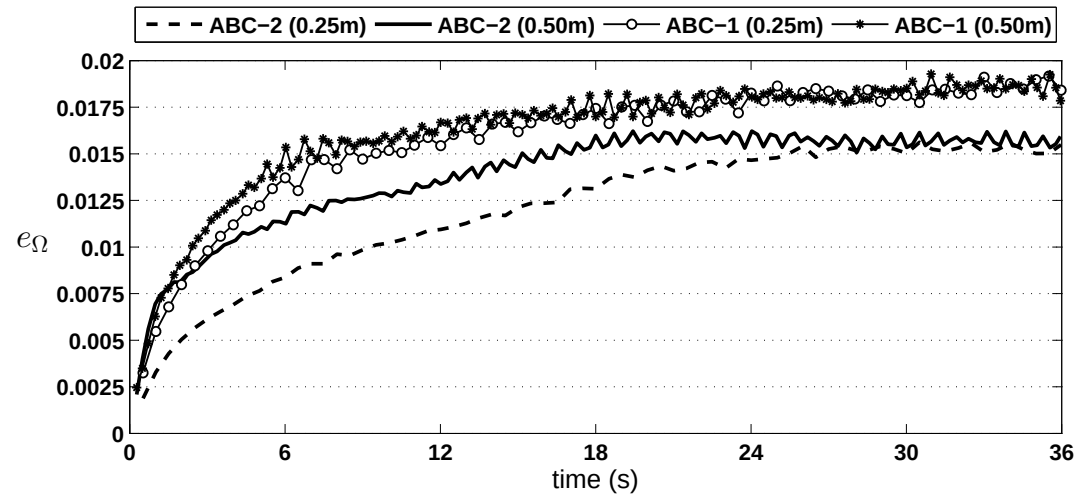

(b) The global norm e_Ω

Figure 10: Error norms $\|e\|_\infty$ (46) and e_Ω (45) as a function of time from the two ABCs on two grid resolutions for the short-crested wave test.

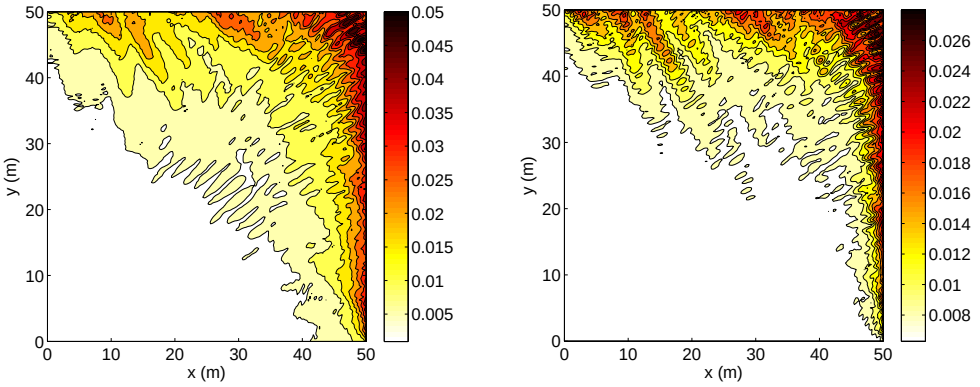

(a) Time-averaged error for ABC-1 (b) Time-averaged error for ABC-2

Figure 11: The pointwise error $|e(i,j)|$ (44) averaged over time for the short-crested wave test on the fine grid with ABC-1 and ABC-2. The error has been scaled with the critical wave height $H_s = 0.1m$ (note the different color scale).

4.2. Circular concentric waves radiating from a localized source

In the second test an oscillating solid sphere with a prescribed motion is impacting on water surface in a tank. The sphere with a radius of 4m is initially located 4m above the free surface, see Fig. 12(a) for the initial condition of the problem. The sphere is allowed to make only vertical motion along the z-direction. Sinusoidal motion of the sphere is prescribed by $z_s(t) = 2 + 2\cos(2.4t)$. After the impact of the sphere on the water surface initially at rest, a series of circular concentric waves is produced radiating outward from the center in all directions. To absorb these waves ABC-1 and ABC-2 are used at the outflow boundaries and their performance is compared. Similar to the previous test reference solution is obtained by repeating the simulation in a large domain, see Fig. 12(b) for the setup of the two domains. The length and the width of Ω_S is the same, $Lx_{\Omega_S} = Ly_{\Omega_S} = 50m$, and its depth is $Lz_{\Omega_S} = 10m$. Ω_L has the same depth but different length and width, $Lx_{\Omega_L} = Ly_{\Omega_L} = 400m$. The size of Ω_L is arranged in such a way that radiating circular waves do not reach the outflow boundaries of Ω_L throughout the simulation.

Two uniform grid resolutions of $0.25m$ and $0.5m$ are considered. Simulations are performed for $30s$. A large number of probes are placed in the domain to compare the free surface elevation records at various locations. Due to the symmetry of the problem we show results only from six probes,

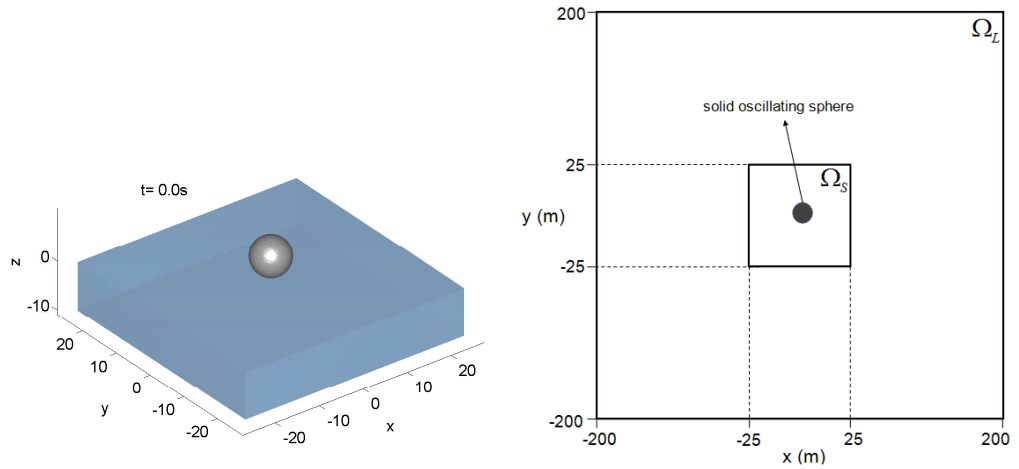

(a) Initial condition of the simulation in Ω_S.

(b) The solution in Ω_L is considered as the reference solution (top view).

Figure 12: Setup for the test with the oscillating solid sphere.

see Fig. 13 for the locations of the probes. Because of the prescribed motion of the sphere the generated circular wave is regular, and both the ABC-1 and ABC-2 are tuned to absorb this regular wave. However, since the wave is circular, it impinges on the outflow boundaries at different angles at different positions. To account for this directional effect, the angle coefficients in both boundary conditions are set to 45°.

Figures 14 and 15 show the free surface elevation history from the six probes on two grid resolutions. As the circular concentric wave travels out from the center, the amplitude of the wave decreases. This is due to the fact that the energy of the wave is spread over a larger area as the wave radiates from the center, which suggests that each particle of the wave gets less energy. This causes a decrease in the wave amplitude. Results demonstrate the superiority of the ABC-2 over ABC-1 clearly. Apart from the wave probe $p\#4$, the other five probes show a significant difference between the performance of the ABC-1 and ABC-2. The probe $p\#4$ is very close the center of the domain, and therefore, it takes more time for the reflected waves to reach this probe. After $t = 25s$ this probe also starts to show some difference. Looking at the peak occurring at $t = 29s$ at the wave probe $p\#1$, the deviations in amplitude with ABC-1 are 42% and 37% on the resolutions of $0.5m$ and $0.25m$, respectively. With ABC-2, however, the deviations are 27%

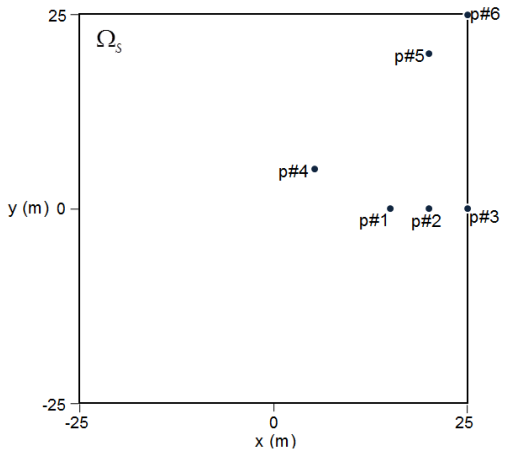

Figure 13: Six wave probes used for comparing the solutions in Ω_S and Ω_L. Positions are $p\#1 = (15m, 0m)$, $p\#2 = (20m, 0m)$, $p\#3 = (25m, 0m)$, $p\#4 = (5m, 5m)$, $p\#5 = (20m, 20m)$, $p\#6 = (25m, 25m)$.

and 9% on the resolutions of $0.5m$ and $0.25m$, respectively. Figure 14 shows that the deviations in amplitude on the resolution of $0.25m$ at $p\#2$ are 58% with ABC-1 and 14% with ABC-2 for the peak occurring at $t = 27.5s$. At $p\#3$ for the peak occurring at $t = 28.7s$, ABC-1 results in a deviation in amplitude of 48% while ABC 21% on the fine grid. The largest deviation in amplitude on the fine grid from ABC-1 is 81% recorded by the wave probe $p\#6$ for the peak occurring at $t = 28.4s$. This value, however, is only 24% with ABC-2. Clearly ABC-1 produces much larger reflection than ABC-2, and the amount of deviation changes considerably between different probes; from 37% at $p\#1$ to 81% at $p\#6$ on the fine grid. However, the deviations caused by ABC-2 vary in a much more limited range; from 9% at $p\#1$ to 24% at $p\#6$ on the fine grid. Similar behaviors from both boundary conditions were observed also in Fig. 10(a).

Fig. 16 illustrates snapshots of the simulations at $t \approx 25s$ when ABC-1 and ABC-2 are used on the fine grid. With ABC-1 different amounts of reflection at different locations result in a chaotic free surface. With ABC-2, however, the free surface is considerably less disturbed.

5. Concluding remarks

This paper presents the design and performance of two absorbing boundary conditions. These boundary conditions are based on the first- and second-

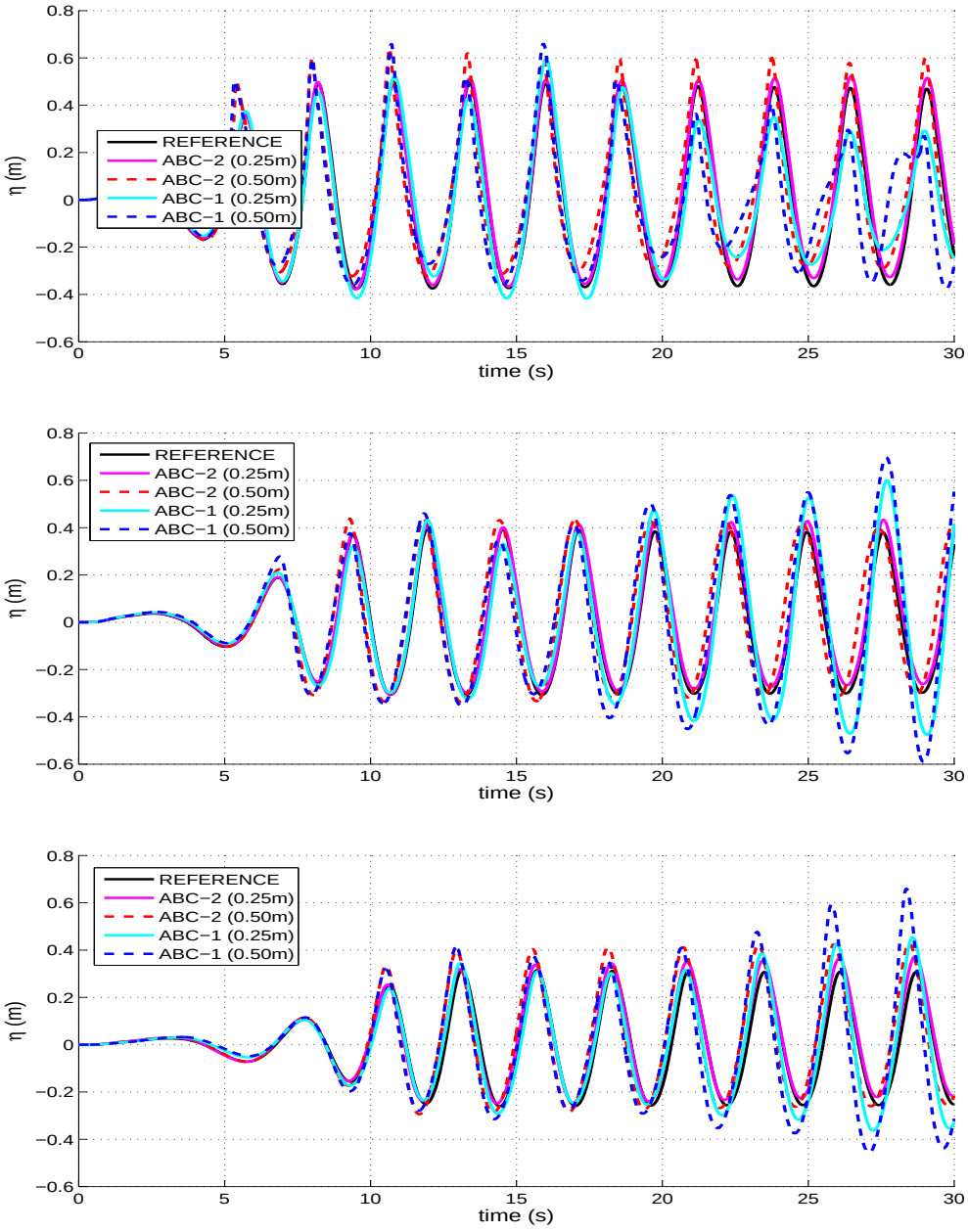

Figure 14: Free surface elevations as a function of time at various locations. From top to bottom results are shown at $p\#1$, $p\#2$ and $p\#3$.

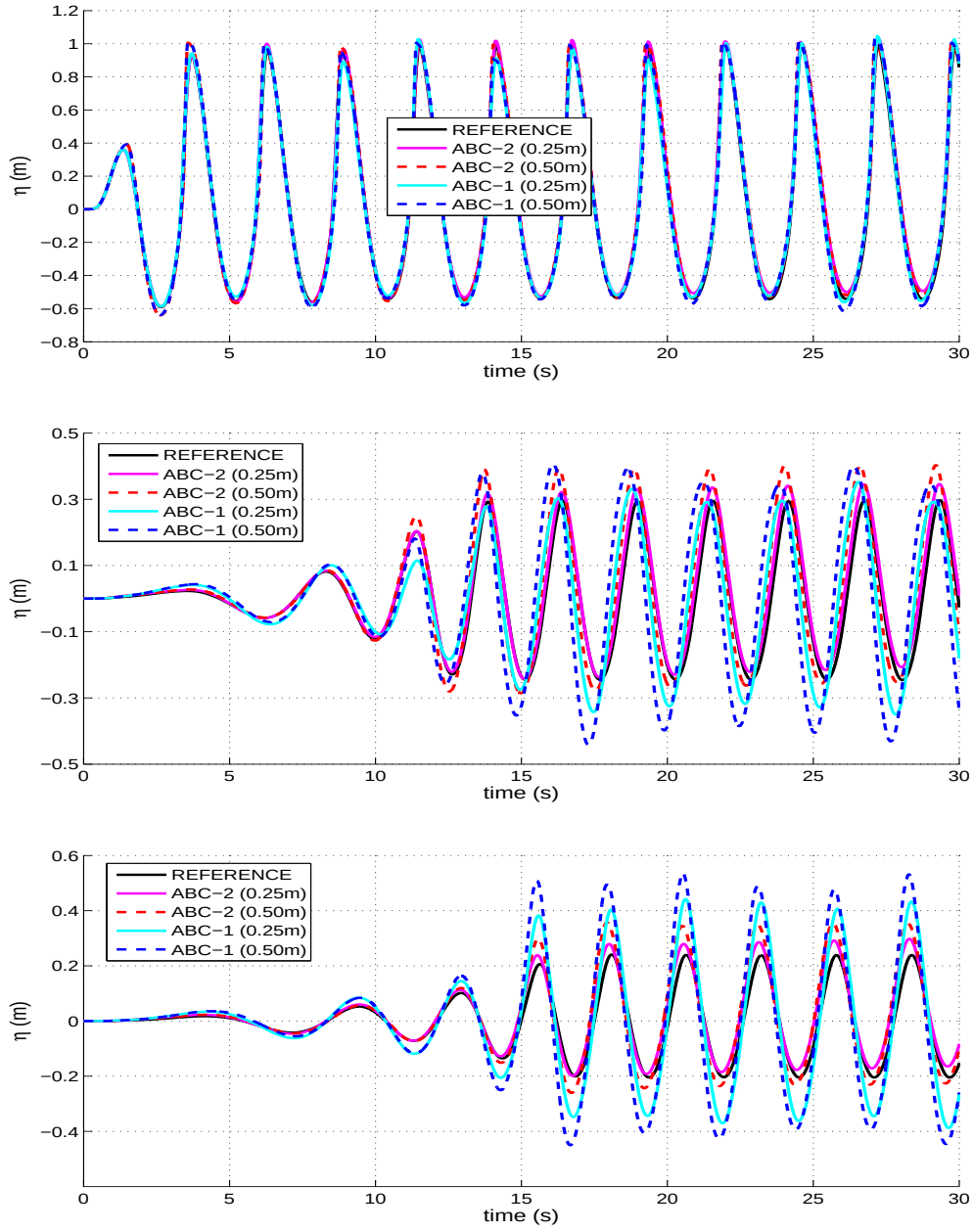

Figure 15: Free surface elevations as a function of time at various locations. From top to bottom results are shown at $p\#4$, $p\#5$ and $p\#6$.

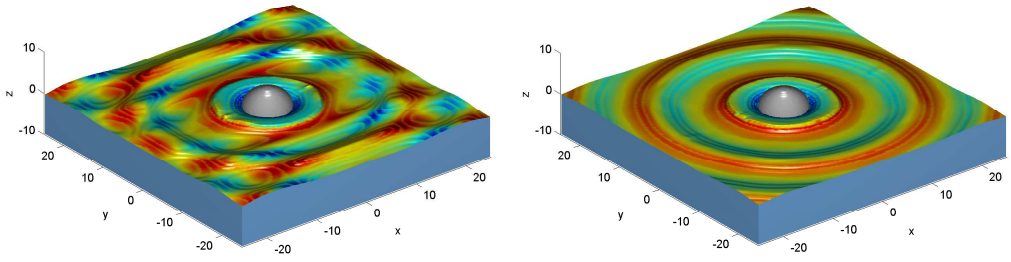

(a) ABC-1 (b) ABC-2

Figure 16: Snapshots of the simulations at $t \approx 25s$ on the fine grid with uniform resolution of $0.25m$ using the two ABCs (colors correspond with the vertical velocity at the free surface).

order Higdon operators [33]. The numerical implementation of the first- and second-order variant, ABC-1 and ABC-2 respectively, using a staggered grid arrangement is explained in detail. Two numerical examples are provided to demonstrate the performance of the ABC-1 and ABC-2. The reflection character is observed, and the results of the computations are discussed and compared. The numerical simulations showed that the second-order variant ABC-2 clearly outperforms the first-order variant ABC-1 in terms of both dispersive and directional effects of waves. Moreover, the increase in performance does not come at the expense of additional computational cost. It was shown that the ABC-2 is solved in the same total number of cells as ABC-1. Compared to that for the ABC-1, the stencil for the ABC-2 is larger and extends in the direction normal to the outflow boundary. Nonetheless, a Krylov subspace solver, BiCGSTAB, with ILU(p) factorization as preconditioner (which was chosen more accurate near the boundaries) was capable enough to solve the linear system within similar amounts of time with ABC-1 and ABC-2.

The proposed ABCs deliver the objectives that were set in the introduction, yet some challenges remain. For example, during the derivation of the ABCs, some assumptions were made; the phase speed of the wave was replaced with the dispersion relation from the linear wave theory, and the temporal derivative of the velocity potential was taken using the linearized Bernoulli equation. Future work will focus on including nonlinear effects so that the ABCs are applicable in a wider range of problems, more particularly, in cases with steep nonlinear waves. Furthermore, the ABCs leave

ample room to include flow currents in their designs; research towards this goal is currently underway.

Acknowledgment
This research is supported by the Dutch Technology Foundation STW, applied science division of NWO and the technology programma of the Ministry of Economic Affairs in The Netherlands (contracts GWI.6433 and 10475).

[1] Appelö, D., 2003. Non-reflecting boundary conditions for wave propagation problems. Ph.D. thesis, Royal Institute of Technology, Sweden.

[2] Bayliss, A., Turkel, E., 1980. Radiation boundary conditions for wave-like equations. Commun Pure Appl Math 33, 707–725.

[3] Berenger, J. P., 1994. A perfectly matched layer for the absorption of electromagnetic waves. J Comput Phys 114, 185–200.

[4] Botta, E. F. F., Ellenbroek, M. H. M., 1985. A modified SOR method for the Poisson equation in unsteady free-surface flow calculations. J. Comput. Phys. 60 (1), 119–134.

[5] Brodtkorb, B., 2008. Prediction of wave-in-deck forces on fixed jacket-type structures based on CFD calculations. In: Proceedings of the 27th international conference on ocean, offshore and arctic eng. OMAE, June 15–20, Estoril (Portugal), vol. 5. pp. 713–721.

[6] Carpenter, K. M., 1982. Note on the paper ′Radiation conditions for the lateral boundaries of limited-area numerical models′ by M.J. Miller, A.J. Thorpe. Quart. J. R. Meteorol. Soc. 108, 717–719.

[7] Chang, X., Akkerman, I., Huijsmans, R. H. M., Veldman, A. E. P., 2016. Generating and absorbing boundary conditions for combined wave-current simulations. In: Proceedings of the 12th Int. Conf. on Hydrodynamics, 18-23 September 2016, Delft (The Netherlands).

[8] Collino, F., 1993. High order absorbing boundary conditions for wave propagation models. Straight line boundary and corner cases. In: Proceedings of the 2nd International Conference on Mathematical and Numerical Aspects of Wave Propagation, SIAM, Delaware (USA). pp. 161–171.

[9] Colonius, T., 2004. Modeling artificial boundary conditions for compressible flow. Annu. Rev. Fluid Mech. 36, 315–345.

[10] Danmeier, D. G., Seah, R. K. M., Finnigan, T., Roddier, D., Aubault, A., Vache, M., Imamura, J. T., 2008. Validation of wave run-up calculation methods for a gravity based structure. In: Proceedings of the 27th Int. Conf. on Ocean, Offshore and Arctic Eng. OMAE, June 15-20 2008, Estoril (Portugal), vol. 6. pp. 265–274.

[11] Durran, D. R., Yang, M. J., Slinn, D. N., Brown, R. G., 1993. Toward more accurate wave-permeable boundary conditions. Mon. Wea. Rev. 121, 604–620.

[12] Düz, B., 2015. Wave generation, propagation and absorption in CFD simulations of free surface flows. Ph.D. thesis, Delft University of Technology, The Netherlands.

[13] Duz, B., Huijsmans, R. H. M., Veldman, A. E. P., Borsboom, M. J. A., Wellens, P. R., 2013. An absorbing boundary condition for regular and irregular wave simulations. in: L. Eça, E. Oñate, J. García-Espinosa, T. Kvamsdal and P. Bergan (Eds.), Computational Methods in Applied Sciences, vol. 29, Springer, pp. 31–45.

[14] Duz, B., Huijsmans, R. H. M., Wellens, P. R., Borsboom, M. J. A., Veldman, A. E. P., 2012. Application of an absorbing boundary condition in a wave-structure interaction problem. In: Proceedings of the 31st Int. Conf. on Ocean, Offshore and Arctic Eng. OMAE, 10-15 June 2012, Rio de Janeiro (Brazil), vol. 5. pp. 863–872.

[15] Engquist, B., Majda, A., 1977. Absorbing boundary conditions for the numerical simulation of waves. Math. Comput. 31, 629–651.

[16] Engsig-Karup, A. P., Bingham, H. B., Lindberg, O., 2009. An efficient flexible-order model for 3D nonlinear water waves. J. Comput. Phys. 228 (6), 2100 – 2118.

[17] Gerrits, J., Veldman, A. E. P., 2003. Dynamics of liquid-filled spacecraft. J. Eng. Math. 45, 21–38.

[18] Givoli, D., 1991. Non-reflecting boundary conditions. J. Comput. Phys. 94, 1–29.

[19] Givoli, D., 2004. High-order local non-reflecting boundary conditions: a review. Wave Motion 39, 319–326.

[20] Givoli, D., 2008. Computational absorbing boundaries. in: S. Marburg and B. Nolte (Eds.), Computational Acoustics of noise propagation in fluids - Finite and boundary element methods, Springer-Verlag, Berlin Heidelberg, pp. 145–166.

[21] Givoli, D., Neta, B., 2003. High-order non-reflecting boundary conditions for dispersive waves. Wave Motion 37, 257–271.

[22] Givoli, D., Neta, B., 2003. High-order non-reflecting boundary scheme for time-dependent waves. J. Comput. Phys. 186, 24–46.

[23] Grote, M. J., Keller, J. B., 1995. Exact nonreflecting boundary conditions for the time dependent wave equation. SIAM J. Appl. Math. 55 (2), 280–297.

[24] Grote, M. J., Keller, J. B., 1996. Nonreflecting boundary conditions for time-dependent scattering. J. Comput. Phys. 127, 52–65.

[25] Grote, M. J., Sim, I., 2009. On local nonreflecting boundary conditions for time dependent wave propagation. Chin. Ann. Math. 30B, 589–606.

[26] Hagstrom, T., 1999. Radiation boundary conditions for the numerical simulation of waves. Acta Numer. 8, 47–106.

[27] Hagstrom, T., Hariharan, S. I., 1998. A formulation of asymptotic and exact boundary conditions using local operators. Appl. Numer. Math. 27, 403–416.

[28] Hagstrom, T., Mar-Or, A., Givoli, D., 2008. High-order local absorbing conditions for the wave equation: Extensions and improvements. J. Comput. Phys. 227, 3322–3357.

[29] Hagstrom, T., Warburton, T., 2004. A new auxiliary variable formulation of high-order local radiation boundary conditions: corner compatibility conditions and extensions to first-order systems. Wave Motion 39, 327–338.

[30] Hedley, M., Yau, M. K., 1988. Radiation boundary conditions in numerical modeling. Mon. Wea. Rev. 116, 1721–1736.

[31] Higdon, R. L., 1986. Absorbing boundary conditions for difference approximations to the multi-dimensional wave equation. Math. Comput. 47, 437–459.

[32] Higdon, R. L., 1986. Initial-boundary value problems for linear hyperbolic systems. SIAM Rev. 28, 177–217.

[33] Higdon, R. L., 1987. Numerical absorbing boundary conditions for the wave equation. Math. Comput. 49, 65–90.

[34] Iwanowski, B., Lefranc, M., Wemmenhove, R., 2009. CFD simulation of wave run-up on a semi-submersible and comparison with experiment. In: Proceedings of the 28th Int. Conf. on Ocean, Offshore and Arctic Eng. OMAE, May 31-June 5 2009, Honolulu (USA), vol. 1. pp. 19–29.

[35] Jensen, T. G., 1998. Open boundary conditions in stratified ocean models. J. Marine Syst. 16, 297–322.

[36] Kleefsman, K. M. T., Fekken, G., Veldman, A. E. P., Iwanowski, B., Buchner, B. A., 2005. A Volume-of-Fluid based simulation method for wave impact problems. J. Comput. Phys. 206, 363–393.

[37] Kreiss, H.-O., 1970. Initial boundary value problems for hyperbolic systems. Comm. Pure Appl. Math. 23, 277–298.

[38] Lancioni, G., 2012. Numerical comparison of high-order absorbing boundary conditions and perfectly matched layers for a dispersive one-dimensional medium. Comput. Methods Appl. Mech. Engrg. 209-212, 74–86.

[39] Lande, O., Johannessen, T. B., 2011. CFD analysis of deck impact in irregular waves: wave representation by transient wave groups. In: Proceedings of the 30th Int. Conf. on Ocean, Offshore and Arctic Eng. OMAE, June 19-24 2011, Rotterdam (Netherlands), vol. 7. pp. 287–295.

[40] Larsen, J., Dancy, H., 1983. Open boundaries in short wave simulations — A new approach. Coastal Engineering 7 (3), 285 – 297.

[41] Loots, G. E., Hillen, B., Veldman, A. E. P., 2003. The role of hemodynamics in the development of the outflow tract of the heart. J. Eng. Math. 45, 91–104.

[42] Mar-Or, A., Givoli, D., 2006. The global-regional model interaction problem: Analysis of Carpenter's scheme and related issues. Int. J. Multiscale Comput. Eng. 4, 617–645.

[43] Mar-Or, A., Givoli, D., 2010. High-order one-way model nesting in dispersive non-uniform media. J. Comput. Appl. Math 234, 1663–1669.

[44] Maurits, N. M., Loots, G. E., Veldman, A. E. P., 2007. The influence of vessel wall elasticity and peripheral resistance on the flow wave form: CFD model compared to in-vivo ultrasound measurements. J. Biomech. 40 (2), 427–436.

[45] Mulder, W. A., 1997. Experiments with Higdon's absorbing boundary conditions for a number of wave equations. Comput. Geosci. 1, 85–108.

[46] Nouri, C., Luppes, R., Veldman, A. E. P., Tuszynski, J. A., Gordon, R., 2008. Rayleigh instability of the inverted one-cell amphibian embryo. Phys. Biol. 5 (1), article 010506.

[47] Orlanski, I., 1976. A simple boundary condition for unbounded hyperbolic flows. J. Comput. Phys. 21, 251–269.

[48] Romate, J. E., 1992. Absorbing boundary conditions for free surface waves. J. Comput. Phys. 99, 135–145.

[49] Sommerfeld, A., 1949. Partial differential equations in physics. Academic Press.

[50] Trefethen, L. N., Halpern, L., 1986. Well-posedness of one-way wave equations and absorbing boundary conditions. Math. Comp. 47, 421–435.

[51] Troch, P., Rouck, J. D., 1999. An active wave generating-absorbing boundary condition for VOF type numerical model. Coast. Eng. 38, 223–247.

[52] Tsynkov, S. V., 1998. Numerical solution of problems on unbounded domains. A review. Appl. Numer. Math. 27, 465–532.

[53] Van Dongeren, A. R., Svendsen, I. A., 1997. Absorbing-generating boundary condition for shallow water models. Journal of Waterway, Port, Coastal, and Ocean Engineering 123 (6), 303–313.

[54] Veldman, A. E. P., 2010. Computational Fluid Dynamics. Lecture notes in Applied Mathematics.

[55] Veldman, A. E. P., Gerrits, J., Luppes, R., Helder, J. A., Vreeburg, J. P. B., 2007. The numerical simulation of liquid sloshing on board spacecraft. J. Comput. Phys. 224, 82–99.

[56] Veldman, A. E. P., Luppes, R., van der Plas, P., van der Heiden, H. J. L., Duz, B., Seubers, H., Helder, J., Bunnik, T., Huijsmans, R. H. M., 2016. Free-surface flow simulations for moored and floating offshore platforms. In: Proceedings of the 7th European Congress on Computational Methods in Applied Sciences and Engineering (ECCOMAS), 5-10 June 2016, Crete Island (Greece).

[57] Veldman, A. E. P., Vogels, M. E. S., 1984. Axisymmetric liquid sloshing under low gravity conditions. Acta Astronaut. 11, 641–649.

[58] Verstappen, R. W. C. P., Veldman, A., 2003. Symmetry-preserving discretization of turbulent flow. J. Comput. Phys. 187, 343–368.

[59] Wei, G., Kirby, J. T., 1995. Time-dependent numerical code for extended Boussinesq equations. J. Waterway, Port, Coastal, Ocean Eng. 121 (5), 251–261.

[60] Wellens, P. R., 2012. Wave simulation in truncated domains for offshore applications. Ph.D. thesis, Delft University of Technology.

[61] Wemmenhove, R., Luppes, R., Veldman, A. E. P., Bunnik, T., 2015. Numerical simulation of hydrodynamic wave loading by a compressible two-phase flow method. Comput. Fluids 114, 218–231.

[62] Zhang, Y., Kennedy, A. B., Panda, N., Dawson, C., Westerink, J. J., 2014. Generating-absorbing sponge layers for phase-resolving wave models. Coastal Engineering 84, 1 – 9.